


## Article

# Implementation of a Two-Source Model for Estimating the Spatial Variability of Olive Evapotranspiration Using Satellite Images and Ground-Based Climate Data

Fernando Fuentes-Peñailillo <sup>1</sup>, Samuel Ortega-Farías <sup>1,\*</sup> , César Acevedo-Opazo <sup>1</sup> and David Fonseca-Luengo <sup>2</sup>

<sup>1</sup> Centro de Investigación y Transferencia en Riego y Agroclimatología (CITRA) and Research Program on Adaptation of Agriculture to Climate Change (A2C2), Universidad de Talca, Casilla 747, Talca 3460000, Chile; ffuentes@utalca.cl (F.F.-P.); cacevedo@utalca.cl (C.A.-O.)

<sup>2</sup> Faculty of Natural Resources, Universidad Católica de Temuco, Temuco 4780000, Chile; dfonseca@uct.cl

\* Correspondence: sortega@utalca.cl; Tel.: +56-71-220-0426

Received: 6 November 2017; Accepted: 16 March 2018; Published: 19 March 2018

**Abstract:** A study was carried out to evaluate the potential use of the two-source Shuttleworth and Wallace (SW) model to compute the intra-orchard spatial variability of actual evapotranspiration (ET) of olive trees using satellite images and ground-based climate data. The study was conducted in a drip-irrigated olive orchard using satellite images (Landsat 7 ETM+), which were acquired on clear sky days during the main phenological stages (2009/10 growing season). The performance of the SW model was evaluated using instantaneous latent heat flux (LE) measurements that were obtained from an eddy correlation system. At the time of satellite overpass, the estimated values of net radiation ( $R_{ni}$ ) and soil heat flux ( $G_i$ ) were compared with ground measurements from a four-way net radiometer and soil heat flux plates, respectively. The results indicated that the SW model subestimated instantaneous LE ( $W\ m^{-2}$ ) and daily ET ( $mm\ d^{-1}$ ), with errors of 12% and 10% of observed values, respectively. The root mean square error (RMSE) and mean absolute error (MAE) values for instantaneous LE were 26 and 20  $W\ m^{-2}$ , while those for daily values of ET were 0.31 and 0.28  $mm\ d^{-1}$ , respectively. Finally, the submodels computed  $R_{ni}$  and  $G_i$  with errors of between 4.0% and 8.0% of measured values and with RMSE and MAE between 25 and 39  $W\ m^{-2}$ .

**Keywords:** crop water requirements; latent heat flux; remote sensing; olive orchard; spatial variability

## 1. Introduction

Better water management of irrigation is required to optimize the water productivity of olive oil production due to water scarcity. Under this scenario, sophisticated irrigation water management will be required to maintain sufficient levels of productivity and quality [1,2]. For these objectives, it is necessary to have an accurate estimation of daily actual evapotranspiration (ET) that is generally computed as a function of reference evapotranspiration ( $ET_0$ ) and crop coefficient ( $K_c$ ) [3]. Several researchers also suggested using the dual crop coefficient approach to describe the ratio of ET to  $ET_0$  by separating  $K_c$  into basal crop coefficient ( $K_{cb}$ ) and soil evaporation coefficient ( $K_e$ ) [3–5]. However, the values of  $K_c$  and  $K_{cb}$  reported in the literature for heteronomous canopies require local adjustment because they depend on canopy architecture and non-linear interaction of soil, cultivar, and climate [1,6,7]. For a hedge-pruned olive orchard, Martínez-Cob and Faci [8] indicated that  $K_c$  values depend on the geometric characteristics of the canopy (canopy shape, distance between trees, etc.) and fractional cover ( $fc$ ). For a super intensive olive orchard, Paço et al. [7] suggested that the  $K_c$  value is affected by several factors, including the canopy

architecture, fractional cover, crop management practices, and rainfall variability. For a drip-irrigated olive orchard, López-Olivari et al. [9] indicated that the ratios of transpiration and evaporation to  $ET_o$  could be significantly affected by the irrigation systems, which determine the percentage of wetted area ( $A_w$ ) of the soil surface. Allen and Pereira [10] and Paço et al. [7] recommended adjusting the  $ET/ET_o$  ratios using  $f_c$  and tree height, according to a density coefficient ( $K_d$ ) that describes the increase in  $K_c$  with an increase in canopy size. Pôças et al. [11] for olive orchard improved the estimation of crop coefficients using remotely sensed vegetation indices and the SIMdualKc soil water balance model. Cammalleri et al. [6] also evaluated a remote sensing-based approach to estimate olive ET, combining a modified version of the standard FAO-56 dual crop coefficient procedure and Penman-Monteith (PM) equation with actual canopy characteristics (i.e., leaf area index, albedo, and canopy height) that were derived from optical remote sensing data. Finally, Er-Raki et al. [12] evaluated the potential of assimilating ET derived from satellite thermal infrared observations to improve the ET simulation performances from the FAO-56 single crop coefficient approach.

Several studies indicated that the two-layer model of Shuttleworth and Wallace (SW) could be used to estimate ET directly without using crop coefficients [13–17]. The SW model can estimate soil evaporation and transpiration separately and has been widely used to estimate ET for homogeneous (sorghum, corn, and wheat) and heterogeneous (vineyards and orchards) canopies [14,18–21]. For heterogeneous canopies, such as vineyards and orchards, the SW approach has been able to estimate ET with errors ranging between 6% and 25%. In a furrow-irrigated vineyard ( $f_c = 0.35$ ), Zhang et al. [20] indicated that the SW model overestimated latent heat flux (LE) with an index of agreement ( $I_a$ ) = 0.75 and a mean absolute error (MAE) =  $39 \text{ W m}^{-2}$ , while Zhang et al. [22] noted that the SW model overestimated ET by 25.2% in a furrow-irrigated vineyard. For drip-irrigated vineyards ( $f_c = 0.30$ ), Ortega-Farías et al. [14] observed that the SW model was able to predict ET with a root-mean-square error (RMSE) =  $0.51 \text{ mm d}^{-1}$  and an MAE =  $0.41 \text{ mm d}^{-1}$ . In a furrow-irrigated vineyard ( $f_c = 0.30$ ), Zhao et al. [23] observed that the SW model estimated ET with a RMSE and MAE of 0.68 and  $0.52 \text{ mm d}^{-1}$ , respectively. In a drip-irrigated olive orchard, Ortega-Farías and Lopez-Olivari [24] observed that the SW model overestimated LE by approximately 2% of measured values, with a RMSE =  $28 \text{ W m}^{-2}$  and  $I_a = 0.98$ . This study also indicated that the SW model was very sensitive to errors in the values of stomatal resistance ( $r_{st}$ ) and leaf area index (LAI). On this matter, Brenner and Incoll [25] indicated that the SW model overestimated crop transpiration of sparsely vegetated shrublands due to the over-estimation of the radiation that is absorbed by the canopy.

The traditional approach of SW model does not consider the effect of intra-orchard spatial variability of soil and canopy vigor on the estimation of ET. Canopy covers of commercial olive orchards are generally incomplete as a result of the canopy geometry that depends on canopy size, leaf area index, and plant density [26]. The canopy training system and associated canopy geometry may significantly affect the partitioning of  $R_n$  into LE, H, or G and thus orchard water requirements. To include the effect of intra-field spatial variability into the SW model, the instantaneous values of net radiation ( $R_{ni}$ ) and soil heat flux ( $G_i$ ) over orchards can be estimated using remote sensing images. In this regard, several studies have suggested that  $R_{ni}$  and  $G_i$  can be adequately estimated in heterogeneous canopies using satellite images. In a drip-irrigated olive orchard, Ortega-Farías et al. [27] indicated that  $R_{ni}$  was estimated with an error of 3% of measured values when using thermal and multispectral images from the Landsat platform. In a drip-irrigated vineyard, Carrasco-Benavides et al. [28] using Landsat 7 images observed that the METRIC model estimated  $R_{ni}$  and  $G_i$  with an error of 11% and 5% of measured values, respectively. However, the estimation of ET from the METRIC model requires the selection of the two “anchor” pixels, which is subjective and depends on the ability of the operator in search and isolate of the most appropriate hot and cold pixels [29–31]. For drip-irrigated olive orchards ( $f_c < 0.3$ ), the selection of the hot and cold pixels is critical because sensible heat flux (H), which is produced at the soil surface, is the main component of energy balance and plays a key role in the tree transpiration and stomatal closure [24].

Dhungel et al. [32] successfully used remote sensing tools to facilitate a comparison of different parameterizations to estimate LE over sparse canopies. This comparison was conducted using gridded weather and Landsat satellite data, such as instantaneous values of ET, surface roughness ( $Z_{om}$ ), emissivity ( $\epsilon_0$ ), albedo ( $\alpha$ ), and leaf area index (LAI), to parameterize the Penman-Monteith (PM) equation. According to our knowledge, there is no available information about the estimation of the intra-orchard spatial variability of olive ET using ground-based weather measurements and remote sensing images as inputs to the SW model. Thus, the main objective of this study is to evaluate the potential use of the two-source SW model to compute the intra-orchard spatial variability of ET of a drip-irrigated olive orchard using satellite images and ground-based climate data. Moreover, the sub-models that were used to estimate the instantaneous values of latent heat flux ( $LE_i$ ), available energy ( $A_i$ ), net radiation ( $Rn_i$ ), and soil heat flux ( $G_i$ ) were also evaluated for the main phenological growth stages of olive trees.

## 2. Materials and Methods

### 2.1. Study Site Description

Measurements were collected in a drip-irrigated commercial olive orchard (*Olea europaea* L. cv Arbequina) that was located in Pencahue, Maule Region, Chile ( $35^{\circ}23'$  S,  $71^{\circ}44'$  W, WGS84, 96 m above sea level) during the 2009–2010 season. The study area has a Mediterranean climate with a medium average temperature of  $14.8^{\circ}\text{C}$  and an accumulated  $ET_0$  of 1013 mm. The average annual rainfall in the region is approximately 602 mm, which is falling mainly during the winter (May to September). The summer period (December to March) is generally hot and dry with a high water vapor pressure deficit. The soil at the experimental site was classified as Quepo series with a clay loam soil. The trees were established using a hedgerow system with 5.0 m between rows and 1.5 m between trees ( $1333\text{ trees ha}^{-1}$ ). The orchard was irrigated by two drippers per tree ( $2.0\text{ L h}^{-1}$ ) spaced at intervals of 0.75 m along the rows. After irrigation, the percentage of wetted area ( $A_W$ ) by the drippers located under the tree canopy was 4.5% of the total area.

To evaluate the irrigation management, the midday stem water potential ( $\Psi_{md}$ ) was measured using a pressure chamber (PMS Instruments Co., Model 1000, Corvallis, OR, USA). A chosen shoot (two per tree, one tree per replicate) containing five to six pairs of leaves was encased in a plastic bag and then wrapped in aluminum foil for (at least) 2 h before being cut [33,34]. In addition, a LI-COR gas analyzer (Li-6400, LI-COR Inc., Lincoln, NE, USA) was used to measure stomatal resistance ( $r_{st}$ ) on two leaves that were directly exposed to the sun and were located on the mid-section of the tree [35]. The  $\Psi_{md}$  and  $r_{st}$  measurements were collected from exposed leaves on 10 trees that were located on both sides of the olive rows. Finally, the LAI was measured weekly using a plant canopy analyzer (LAI-2000, LI-COR, Lincoln, NE, USA), which was calibrated according to Lopez-Olivari et al. [9]. Also, it is important to indicate that  $\Psi_{md}$  and  $r_{st}$  were measured at the time of satellite overpass.

### 2.2. Measurements of Climate and Energy Balance Data

Two towers (4.8 m height) were installed on a flat and homogeneous plot (6.45 ha) in an olive orchard to measure the surface energy balance components and micrometeorological variables at intervals of 30 min. Hobo sensors (Onset Computer, Inc., Bourne, MA, USA) were used to measure relative humidity (RH) and air temperature ( $T_a$ ). An anemometer (03101-5, R. M. Young Co., Traverse City, MI, USA) and a pluviometer (A730RAIN, Adcon Telemetry, Klosterneuburg, Austria) were used to measure wind speed ( $u$ ) and precipitation ( $P_p$ ), respectively. The net radiation ( $Rn$ ) was measured with a four-way net radiometer (CNR1, Kipp & Zonen, Delft, The Netherlands). Finally, the sensors to measure  $u$ ,  $P_p$ ,  $T_a$ , RH, and  $Rn$  were located at 1.9 m above the tree canopy.

Soil heat flux was estimated through the use of eight flux plates installed on either side of the rows (four plates in the inter row and four plates below the row). This arrangement considers the row shade effect throughout the day [36]. The flux plates with a constant thermal conductivity (HFT3,

Campbell Sci., Logan, UT, USA) were installed at a depth of 0.08 m. Additionally, two averaging thermocouple probes (TCAV, Campbell Sci., Logan, UT, USA) that were used to measure soil temperature were installed above each flux plate at depths of 0.02 and 0.06 m. All of the thermocouple probe signals were recorded on an electronic datalogger (CR3000, Campbell Sci, Logan, UT, USA) with a thirty-minute interval. Finally, soil heat flux was calculated at each position by adding the measured flux at 0.08 m to the heat that was stored in the layer above the heat flux plates [9,37].

The latent (LE) and sensible (H) heat fluxes were measured with an eddy covariance (EC) system, which is composed of a three-dimensional sonic anemometer (CSAT3, Campbell Scientific Inc., Logan, UT, USA) and an infrared gas analyzer (LI-7500, LI-COR Inc., Lincoln, NE, USA). The fluxes were registered at 1.6 m above the canopy at intervals of 10 Hz and were stored on a data logger (CR5000, Campbell Scientific Inc., Logan, UT, USA). Finally, a post-processing step was conducted to correct the sonic temperature due to crosswind influences [38] and water vapor density due to the influences of the fluctuations in temperature and humidity [39].

To reduce the uncertainty that is associated with the errors in the LE and H measurements, entire days were excluded from the study when the ratios of (H + LE) to (Rn − G) were outside the range between 0.8 and 1.2 [9]. Assuming that the measurements of Rn and G were representative of the available energy over the olive orchard, the fluxes of H and LE were forced to close the energy balance using the Bowen ratio approach ( $B = H/LE$ ) [8,24,36,40]:

$$LE_B = \frac{(Rn - G)}{(1 + B)} \quad (1)$$

$$H_B = \frac{(Rn - G)}{(1 + B^{-1})} \quad (2)$$

On a daily basis, the olive ET was calculated, as follows:

$$ET_{EC} = \frac{\sum_{n=1}^{24} LE_{B,n}}{\lambda \rho_w} 1.8 \quad (3)$$

where  $ET_{EC}$  is the actual evapotranspiration of the olive orchard measured by the EC system ( $\text{mm d}^{-1}$ ), 1.8 is a conversion factor,  $\lambda$  is the latent heat of vaporization ( $1013 \text{ MJ kg}^{-1}$ ),  $\rho_w$  is the water density ( $1000 \text{ kg m}^{-3}$ ), and  $n$  is the number of measurements during a 24-h period. The subscript B indicates that turbulent fluxes were recalculated using the Bowen ratio approach.

### 2.3. Shuttleworth and Wallace Model Description

At the time of satellite overpass, the SW model can estimate latent heat flux over olive orchards as the sum of the Penman-Monteith equation for evaporation and transpiration weighted by a set of coefficients that account for the combination of soil and canopy resistances. This can be done as follows [41]:

$$LE_i = T_i + E_i \quad (4)$$

$$T_i = C_c \frac{\Delta A_i + \left( \frac{\rho_a C_p D_i - \Delta r_a^c A_{si}}{r_a^a + r_a^c} \right)}{\Delta + \gamma \left( 1 + \frac{r_s^c}{(r_a^a + r_a^c)} \right)} \quad (5)$$

$$E_i = C_s \frac{\Delta A_i + \left( \frac{\rho_a C_p D_i - \Delta r_a^s (A_i - A_{si})}{r_a^a + r_a^s} \right)}{\Delta + \gamma \left( 1 + \frac{r_s^s}{(r_a^a + r_a^s)} \right)} \quad (6)$$

where  $LE_i$  is the instantaneous latent heat flux computed from the SW model ( $\text{W m}^{-2}$ ),  $T_i$  is the latent heat flux from the tree transpiration ( $\text{W m}^{-2}$ ),  $E_i$  is the latent heat flux from soil evaporation ( $\text{W m}^{-2}$ ),  $C_c$  is the canopy resistance coefficient (dimensionless),  $C_s$  is the soil surface resistance coefficient

(dimensionless),  $\Delta$  is the slope of the saturation vapor pressure curve at the mean temperature ( $\text{kPa } ^\circ\text{C}^{-1}$ ),  $A_i$  is the available energy leaving the complete canopy ( $\text{W m}^{-2}$ ),  $A_{Si}$  is the available energy at the soil surface ( $\text{W m}^{-2}$ ),  $C_p$  is the specific heat of the air at a constant pressure ( $1013 \text{ J kg}^{-1} \text{ K}^{-1}$ ),  $D_i$  is the water vapor pressure deficit at the reference height ( $\text{kPa}$ ),  $r_a^c$  is the bulk boundary layer resistance of the vegetative elements in the canopy ( $\text{s m}^{-1}$ ),  $r_a^a$  is the aerodynamic resistance between the canopy source height and reference level ( $\text{s m}^{-1}$ ),  $\gamma$  is the psychrometric constant ( $\text{kPa } ^\circ\text{K}^{-1}$ ),  $r_s^c$  is the canopy resistance ( $\text{s m}^{-1}$ ),  $r_a^s$  is the aerodynamic resistance between the soil and canopy source height ( $\text{s m}^{-1}$ ), and  $r_s^s$  is the soil surface resistance ( $\text{s m}^{-1}$ ). Subscripts “i” denote the values that are computed at the time of satellite overpass.

#### 2.4. Estimation of Resistances

Values of  $r_s^c$  and  $r_a^c$  are calculated as:

$$r_s^c = \frac{r_{st}}{\text{LAI}} \quad (7)$$

$$r_a^c = \frac{r_b}{\text{LAI}} \quad (8)$$

where  $r_{st}$  is the mean stomatal resistance ( $\text{s m}^{-1}$ ),  $r_b$  is the mean boundary layer resistance ( $\text{s m}^{-1}$ ) and LAI is the leaf area index ( $\text{m}^2 \text{ m}^{-2}$ ). For this study,  $r_b$  was assumed to be equal to  $25 \text{ s m}^{-1}$ , and a constant value of  $r_s^s = 2000 \text{ s m}^{-1}$  was used because of the dryness of the soil surface (between rows) during the study periods [41]. Additionally, a mean value of measured  $r_{st} = 235 (\pm 60.84) \text{ s m}^{-1}$  was used for the simulation period. Finally, general descriptions of  $r_a^a$ ,  $r_a^s$ ,  $C_s$ , and  $C_c$  can be found in Shuttleworth and Wallace [41] and Ortega-Farías et al., 2007 [21].

#### 2.5. Estimation of Available Energy at the Time of the Satellite Overpass

The instantaneous values of available energy over the canopy ( $A_i$ ) and soil surface ( $A_{Si}$ ) can be calculated as:

$$A_i = \text{Rn}_i - G_i \quad (9)$$

$$A_{Si} = \text{Rn}_{Si} - G_i \quad (10)$$

where  $\text{Rn}_i$  is the net radiation ( $\text{W m}^{-2}$ ),  $G_i$  is the soil heat flux ( $\text{W m}^{-2}$ ) and  $\text{Rn}_{Si}$  is the net radiation on the surface of the ground ( $\text{W m}^{-2}$ ), which can be calculated using Beer’s law, through the next expression:

$$\text{Rn}_{Si} = \text{Rn}_i \times \exp(-C \times \text{LAI}) \quad (11)$$

where  $C$  is the extinction coefficient of the net radiation of the crop (dimensionless). In this study, a mean value of measured  $\text{LAI} = 1.29 (\pm 0.07)$  was used as a constant while  $C$  was assumed to be 0.66 [24]. Values of  $\text{Rn}_i$  were obtained, as follows [42]:

$$\text{Rn}_i = (1 - \alpha_i) \times R_{s\downarrow} + R_{L\downarrow} - R_{L\uparrow} - (1 - \varepsilon_0) \times R_{L\downarrow} \quad (12)$$

where  $\alpha_i$  is the surface albedo,  $R_{s\downarrow}$  is the short-wave incident radiation ( $\text{W m}^{-2}$ ),  $R_{L\downarrow}$  and  $R_{L\uparrow}$  are the incoming and outgoing long-wave radiation, respectively, and  $\varepsilon_0$  corresponds to the superficial emissivity. The values of  $R_{L\downarrow}$  and  $R_{L\uparrow}$  were obtained as:

$$R_{L\uparrow} = \varepsilon_0 \times \sigma \times T_s^4 \quad (13)$$

$$R_{L\downarrow} = \varepsilon_a \times \sigma \times T_a^4 \quad (14)$$

where  $\sigma$  is the Stefan-Boltzmann constant ( $5.67 \times 10^{-8} \text{ W m}^{-2} \text{ K}^{-4}$ ),  $T_s$  is the superficial temperature ( $^\circ\text{K}$ ),  $\varepsilon_0$  is the “broad-band” surface emissivity (dimensionless),  $T_a$  is the near-surface air temperature ( $^\circ\text{K}$ ), and  $\varepsilon_a$  is the effective atmospheric emissivity (dimensionless). The methodologies to estimate  $\varepsilon_0$ ,  $\varepsilon_a$ , and  $T_s$  are indicated by Allen et al. [42].

$G_i$  was calculated using the following empirical relation [26]:

$$G_i = 0.3236 \times Rn_i - 51.52 \quad (15)$$

## 2.6. Instantaneous to Daily Extrapolation of Actual Evapotranspiration

Using multispectral and thermal images from the Landsat satellite and ground-based weather data, the daily ET was computed for each image pixel using the following equations [28,42]:

$$ET_i = 3600 \frac{LE_i}{\rho_w \lambda} \quad (16)$$

$$E_F = \frac{ET_i}{ET_{oi}} \quad (17)$$

$$ET_{sw} = E_F \times ET_o \quad (18)$$

where  $ET_i$  is the instantaneous ET computed from the SW model ( $\text{mm h}^{-1}$ ),  $\rho_w$  is the density of water ( $1000 \text{ kg m}^{-3}$ ),  $\lambda$  is the latent heat of vaporization ( $\text{J kg}^{-1}$ ),  $ET_{oi}$  is the instantaneous reference evapotranspiration ( $\text{mm h}^{-1}$ ),  $ET_{sw}$  is the daily actual evapotranspiration estimated using the SW model ( $\text{mm d}^{-1}$ ),  $ET_o$  is the daily reference evapotranspiration ( $\text{mm d}^{-1}$ ), and  $E_F$  is the reference evapotranspiration fraction.

## 2.7. Image Processing

Seven Landsat (7 ETM+) satellite images were downloaded from the USGS GloVis web platform for free (<http://glovis.usgs.gov>) using the coordinates WRS-2 Path/Row: 233/85 (Table 1). The SLC instrument suffered a problem in 2003; thus, the images have lines of pixels without information. A method that was proposed by Storey et al. [43] was implemented to fill the pixels without data. This method estimates the value of the pixel based on the neighboring pixels in an image taken on a similar date. The estimations present good results in most of the images, but not in images with abrupt temporal transitions [44]. Also, the image processing for satellite information considered the methodology that was proposed by Allen et al. [42], aiming to generate radiometric and atmospheric corrections.

**Table 1.** Images selected for processing the Shuttleworth and Wallace model (SW) and main phenological stages of a drip-irrigated olive orchard.

Date	Day of Year	Overpass Time	Scene Cloud Cover	Phenological Stages
(dd-mm-yy)	(DOY)	(UTC)	(%)	
4/02/2009	35	2:24:02 p.m.	1	FC
20/02/2009	51	2:24:12 p.m.	2	FC
3/11/2009	307	2:24:42 p.m.	7	F
5/12/2009	339	2:25:05 p.m.	21	FS
21/12/2009	355	2:25:21 p.m.	1	PH
6/01/2010	6	2:25:38 p.m.	1	PH
22/01/2010	22	2:25:52 p.m.	0	PH

F = flowering; FS = fruit set; PH = pit hardening; FC = fruit colouring.

Multispectral and thermal data from each satellite image were processed pixel by pixel to estimate  $LE_i$ ,  $Rn_i$ ,  $G_i$ , and  $ET_i$ . In this regard, the satellite images were obtained from November to February where the main phenological periods were observed in the drip-irrigated olive orchard (Table 1). Finally, it is important to indicate that the number of days with a complete data set (satellite images and EC fluxes) was limited by cloudiness when the satellite overpassed the experimental site and persistent noise of the EC system (instrumental problems and flow distortion through the tower). For these



reasons, several researchers have used a limited number of images to evaluate the satellite-based remote sensing (SBRS) models [6,45–49].

## 2.8. Statistical Analysis

The SW model used to compute the instantaneous latent heat flux ( $LE_i$ ) and daily actual evapotranspiration ( $ET_{sw}$ ) was validated using ground-based weather measurements. The validation was carried out using the ratio of the estimated to observed values ( $b$ ), root-mean-square error (RMSE), mean absolute error (MAE), and index of agreement ( $I_a$ ) [50,51]. The  $t$ -test was used to determine whether the  $b$  value was significantly different from unity at the 95% confidence level. In addition, the sub-models for estimating  $A_i$ ,  $Rn_i$ , and  $G_i$  were included in the validation. Values of RMSE, MAE, and  $I_a$  were computed, as follows:

$$RMSE = \left[ N^{-1} \sum_{i=1}^N (P_i - O_i)^2 \right]^{0.5} \quad (19)$$

$$MAE = N^{-1} \sum_{i=1}^N |P_i - O_i| \quad (20)$$

$$I_a = 1 - \left[ \frac{\sum_{i=1}^N (P_i - O_i)^2}{\sum_{i=1}^N (|P_i - \bar{O}| + |O_i - \bar{O}|)^2} \right] \quad 0 \leq I_a \leq 1 \quad (21)$$

where  $N$  is the total number of observations,  $P_i$  and  $O_i$  are the estimated and observed values, respectively, and  $\bar{O}$  is the mean of the observed values. Values of RMSE, MAE,  $P_i$ ,  $O_i$ , and  $\bar{O}$  are in  $W m^{-2}$  or  $mm d^{-1}$

Finally, a sensitivity analysis of the inputs parameters ( $C$ ,  $d$ ,  $LAI$ ,  $n$ ) and resistances ( $r_b$ ,  $r_{st}$ ,  $r_a^a$ ,  $r_a^c$ ,  $r_a^s$ ) was conducted to evaluate their effects on the ability of the SW model for estimating  $ET_i$ . In this case, the percent deviation of the mean  $ET_i$  was computed when the input values of the parameters and resistances individually varied by  $\pm 30\%$ .

## 3. Results

The atmospheric conditions were very dry and hot during the main phenological periods (FS, PH, and FC) of the olive orchard, which were observed from December to February (Table 1). During this period, the values of  $u$ ,  $T_a$  and  $D$  were between  $0.3$  and  $4.5 m s^{-1}$ ,  $28.3$ – $13.4 ^\circ C$ , and  $0.2$ – $2.9 kPa$ , respectively (Figure 1a,b). During the study, four rainfall events were observed with values of less than  $5 mm$ . The accumulated value of  $ET_o$  from September to March (growing season) was  $907 mm$  while that from December to March (summer) was  $616 mm$ . During this study, the average values of  $ET_o$  and  $ET_{oi}$  were  $6.95 (\pm 0.99) mm d^{-1}$  and  $0.58 (\pm 0.06) mm h^{-1}$ , respectively (Table 2). These results indicate that the drip-irrigated olive orchard was under high atmospheric demand for water vapor (Figure 1). Under this atmospheric condition, values of  $\Psi_{md}$  ranged between  $-1.37$  and  $-1.49 MPa$ , indicating that olive trees were well irrigated during the main phenological periods (F, FS, PH, and FD). Finally, Figure 1 shows that clear days were observed when the satellite passed over the experimental site.

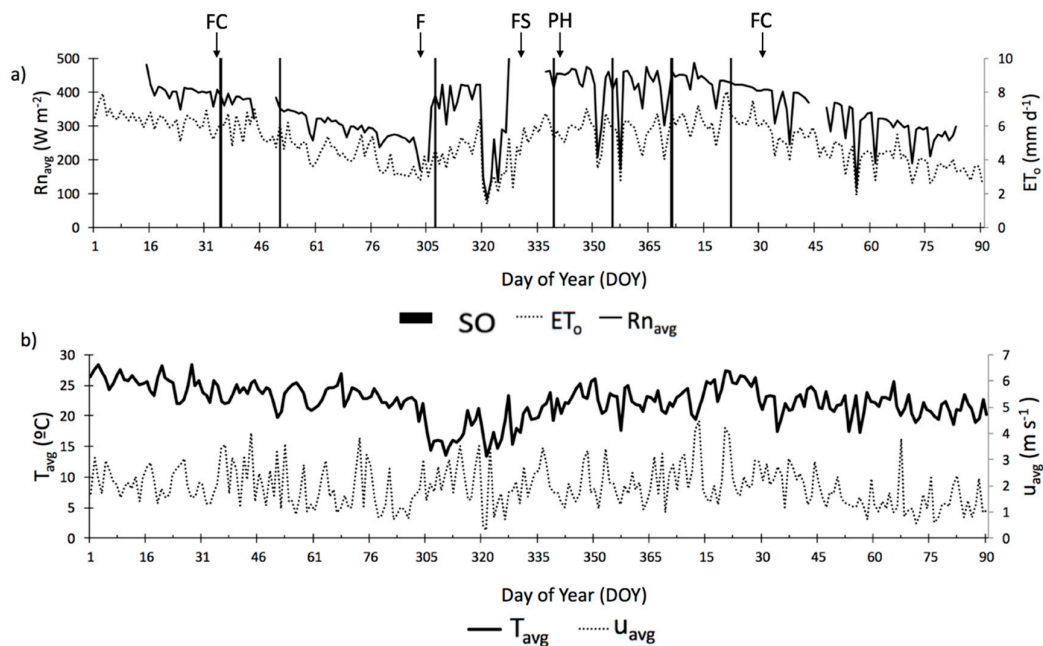


**Figure 1.** (a) Daily variation of net radiation ( $Rn_{avg}$ ) and reference evapotranspiration ( $ET_o$ ); (b) average daily values of temperature ( $T_{avg}$ ) and average daily values of wind speed ( $u_{avg}$ ). The vertical bars indicate the time of satellite overpass (SO). Also, phenological stages are indicated by an abbreviation followed by an arrow where F = flowering, FS = fruit Set, PH = pit hardening and FC = fruit colouring.

**Table 2.** Meteorological conditions during the study period.

DOY	Date	$ET_o$	$ET_{oi}$	RH	Ta	U
		( $mm d^{-1}$ )	( $mm h^{-1}$ )	(%)	( $^{\circ}C$ )	( $m s^{-1}$ )
35	4/02/2009	7.88	0.56	51.94	22.91	0.81
51	20/02/2009	6.88	0.52	54.16	17.92	4.11
307	3/11/2009	5.13	0.54	58.85	14.12	2.33
339	5/12/2009	6.47	0.57	56.12	16.36	1.17
355	21/12/2009	6.69	0.69	47.6	21.29	2.69
6	6/01/2010	7.84	0.6	53.53	21.33	2.69
22	22/01/2010	7.75	0.61	52.99	22.17	1.29
	Mean	6.95	0.58	53.6	19.44	2.16
	D.E.	0.99	0.06	3.5	3.33	1.15

where  $ET_o$  = daily reference evapotranspiration,  $ET_{oi}$  = instantaneous reference evapotranspiration, RH = Relative air humidity, Ta = Air Temperature and u = wind speed.

At 30 min time intervals, the ratio of  $(Rn - G)$  to  $(H + LE)$  was 0.89, suggesting that the orchard energy balance (SEB) was systematically imbalanced by approximately 11% (Figure 2). Several researchers reported a similar situation where the values of  $(LE + H)$  were less than those of  $(Rn - G)$  above olive orchards when the EC technique was used. In flood-irrigated olive orchards, Williams et al. [52], Ezzahar et al. [53], and Er-Raki et al. [4] reported imbalances ranging between 9% and 26%, while in drip-irrigated olive orchards, Villalobos et al. [54] and Testi et al. [55] indicated imbalances varying between 5% and 17%. The potential errors can be attributed to the uncertainties in the measurements of  $Rn$  and  $G$  [56–58], and energy storage within the olive tree biomass [9,53]. In this case, Twine et al. [40] suggested that  $LE$  and  $H$  values from the EC system can be corrected using the Bowen ratio ( $\beta = H/LE$ ) because the different problems affect the measured values of  $H$  and  $LE$  in a similar proportion. Using this correction, however, Allen et al. [59] indicated that the lack of closure can be only attributed to errors in the measurements of  $H$  and  $LE$  without considering the potential



bias in  $R_n - G$ . According to several researchers, the uncertainties observed in this study are modest and turbulent fluxes were recalculated using the Bowen-ratio approach [8,24,36,40,60].

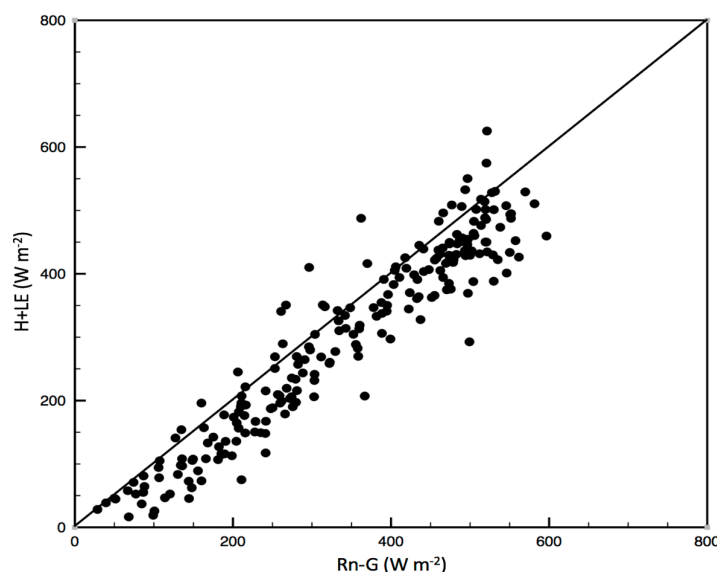


**Figure 2.** Energy balance closure at interval of 30 min for the days when the satellite overpassed the experimental site.  $H$ ,  $LE$ ,  $R_n$ , and  $G$  correspond to sensible heat flux ( $W m^{-2}$ ), latent heat flux ( $W m^{-2}$ ), net radiation ( $W m^{-2}$ ), and soil heat flux ( $W m^{-2}$ ), respectively. The coefficient of determination ( $R^2$ ) was 0.88 and the  $(R_n - G)/(H + LE)$  ratio was 0.89.

### 3.1. Model Validation of Available Energy, Latent Heat Flux and Actual Evapotranspiration

The model validation of  $R_{ni}$ ,  $G_i$ , and  $A_i$  is indicated in Table 3 when using ground-based weather measurements and satellite images. The results indicated that the sub-model was able to predict values of  $A_i$  with a  $RMSE = 25 W m^{-2}$  and  $MAE = 21 W m^{-2}$ . The  $RMSE$  and  $MAE$  values for  $R_{ni}$  were between 39 and 32  $W m^{-2}$ , while those for  $G_i$  were between 33 and 27  $W m^{-2}$ , respectively (Table 3). The  $t$ -test showed that the  $b$  values were different from unity, indicating that  $A_i$ ,  $R_{ni}$ , and  $G_i$  were underestimated, with errors ranging between 4% and 8% of observed values in the drip-irrigated olive orchard. Finally, the comparison between the measured and modeled values in Figure 3 shows that all points were close to the 1:1 line, suggesting a good performance of the sub-models to estimate  $A_i$ ,  $R_{ni}$ , and  $G_i$ . For  $R_{ni}$  and  $G_i$ , the results that were observed in this study are similar to those that are found in literature for heterogeneous canopies, such as orchards and vineyard. For winegrape (drip irrigated) and table grape (micro sprinkler), Teixeira et al. [61] observed values of coefficient of determination ( $R^2$ ) = 0.94 and  $RMSE = 17.5 W m^{-2}$  for  $R_{ni}$  when using satellite images (Landsat 5 and 7). For a drip-irrigated olive orchard ( $fc = 0.29$ ), Ortega-Farías et al. [27] found that the METRIC model underestimated  $R_{ni}$  by approximately 3% of the observed values, with  $RMSE$  and  $MAE$  values of 40 and 33  $W m^{-2}$ , respectively. In a super intensive olive orchard ( $fc = 0.3$ ), Ortega-Farías et al. [26] indicated that the model was able to estimate  $R_{ni}$  and  $G_i$ , with errors of 5% and 2%, respectively, when using high-resolution thermal and multispectral data acquired with an unmanned aerial vehicle (UAV). In a drip-irrigated vineyard ( $fc = 0.3$ ), Carrasco-Benavides et al. [28] noted that the METRIC model was able to estimate  $R_{ni}$  and  $G_i$ , with errors of 11% and 5%, respectively. In an experiment that was carried out using remote sensing techniques over heterogeneous landscapes, Liu et al. [62] found  $RMSE$  and  $MAE$  values of 51 and 25  $W m^{-2}$ , respectively, when  $G_i$  was evaluated.

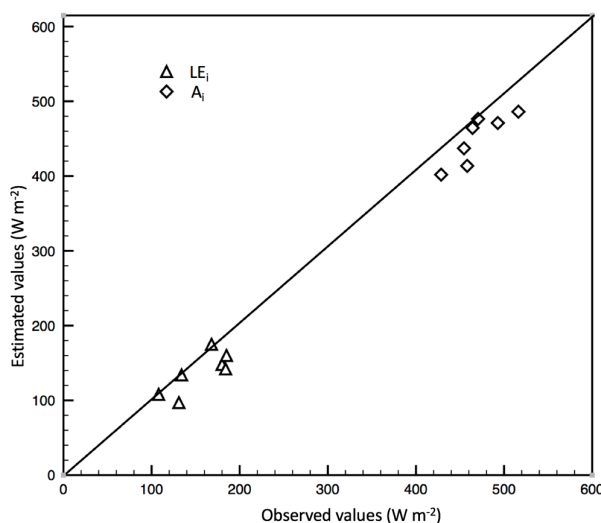


**Figure 3.** Comparison between estimated and observed values of instantaneous latent heat flux ( $LE_i$ ) from the two-source model and instantaneous available energy ( $A_i$ ) at the time of satellite overpass. Values of index of agreement (d) for  $LE_i$  and  $A_i$  were 0.8 and 0.82, respectively.

**Table 3.** Model validation of instantaneous values of net radiation ( $Rn_i$ ), soil heat flux ( $G_i$ ), available energy ( $A_i$ ), and latent heat flux ( $LE_i$ ) over a drip irrigated olive orchard. Also, daily actual evapotranspiration ( $ET_{SW}$ ) is included in the analysis.

Variable	RMSE	MAE	$I_a$	b	t-Test
$Rn_i$ ( $W\ m^{-2}$ )	39	32	0.79	0.96	F
$G_i$ ( $W\ m^{-2}$ )	33	27	0.5	0.92	F
$A_i$ ( $W\ m^{-2}$ )	25	21	0.82	0.96	F
$LE_i$ ( $W\ m^{-2}$ )	26	20	0.8	0.88	F
$ET_{SW}$ ( $mm\ d^{-1}$ )	0.31	0.28	0.95	0.90	F

where RMSE = Root mean square error, MAE = Mean absolute error, b = Ratio of estimated to observed values and  $I_a$  = Index of agreement. T = null hypothesis (b = 1) True; F = alternative hypothesis (b  $\neq$  1).

Table 3 indicates that the SW model underestimated  $LE_i$  by approximately 12% of observed values, with RMSE =  $26\ W\ m^{-2}$  and MAE =  $20\ W\ m^{-2}$  (Table 3). In addition, the comparisons between the observed and estimated values of LE at the time of satellite overpass show that most of the points are close to the 1:1 line (Figure 3). Furthermore, the model validation indicated the SW model was able to simulate the ET with RMSE and MAE values that are equal to 0.31 and  $0.28\ mm\ d^{-1}$ , respectively (Table 3). Additionally, the statistical analysis indicated that the ratio of  $ET_{SW}/ET_{EC}$  was significantly different from unity, suggesting that the SW model underestimated ET with an error of 10% of observed values. In this regard, Figure 4 shows that all of the points were distributed below the 1:1 line. In a super intensive olive orchard ( $fc = 0.3$ , LAI = 1.3), Ortega-Farías and Lopez-Olivari [24] indicated that the SW model overestimated  $LE_i$  and ET by approximately 2% and 6% of observed values, respectively, suggesting that the model was very sensitive to errors in the estimation of  $r_{st}$  and LAI. Finally, in a furrow-irrigated vineyard ( $fc = 0.35$ , IAF = 2), Zhang et al. [20] observed MAE values about of  $39\ W\ m^{-2}$  when SW model was evaluated.

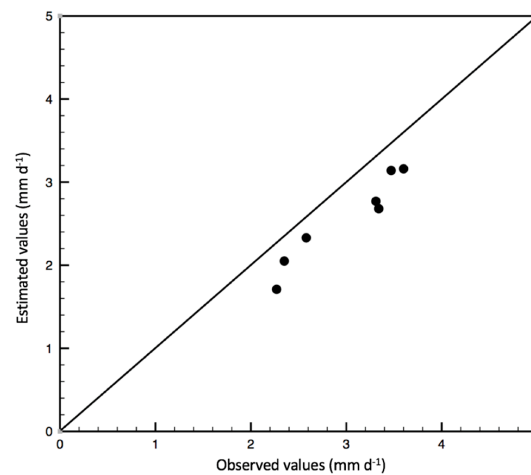


**Figure 4.** Comparison between estimated and observed values of daily actual evapotranspiration of a drip irrigated olive orchard. ( $ET_{SW}$ ). Index of agreement ( $I_a$ ) for  $ET_{SW}$  was equal to 0.95. This comparison was done using days when satellite images were available.

### 3.2. Sensitivity Analysis

Table 4 indicates that when  $Rn_i$  varied by  $\pm 30\%$ , a variation of  $\pm 20\%$  was observed in the estimation of  $ET_i$ . Also, the results indicated that the sensitivity of the predicted  $ET_i$  in respect to the uncertainties in  $C$ ,  $d$ ,  $n$ , and  $r_b$  was minimal. In addition, the sensitivity analysis indicated that the estimation of  $ET_i$  was significantly affected by variations of  $\pm 30\%$  in the values of LAI and  $r_s^c$ . In this regard, the values of  $ET_i$  varied between  $+15\%$  and  $-14\%$  and between  $-13\%$  and  $+20\%$  when LAI and  $r_s^c$  varied by  $\pm 30\%$ , respectively. (Table 4). This sensitivity analysis suggests that the  $ET_i$  that was estimated using the SW model was very sensitive to  $Rn_i$ , LAI, and  $r_{st}$ , but it was not sensitive to errors in the estimations of  $r_a^a$ ,  $r_a^c$ , and  $r_a^s$ . Similar results in a drip-irrigated olive orchard were observed by Ortega-Farías and Lopez-Olivari [24], who indicated that the ET predicted by the SW model was sensitive to errors of  $\pm 30\%$  in LAI and  $r_{st}$ , but was not significantly affected by errors in the estimation of aerodynamic resistances. Therefore, correct estimations of  $Rn_i$ , LAI and  $r_{st}$  become critical to increasing the accuracy of the SW model.

**Table 4.** Sensitivity analysis to instantaneous actual evapotranspiration ( $ET_i$ ).

Variables	Symbol	Parameters	30%	−30%
Extinction coefficient of crop for net radiation (dimensionless)	C	0.66 *	0.09	0.53
Zero plane displacement of crop with complete canopy cover (LAI = 4) (m)	d	2.01 *	−0.26	3.29
Leaf Area Index ( $m^2 m^{-2}$ )	LAI	1.29 *	13.93	−14.52
Eddy diffusivity decay constant in crop with complete canopy crop cover (dimensionless)	n	2.5 *	2.16	−0.95
Mean boundary layer resistance per unit area of vegetation ( $s m^{-1}$ )	$r_b$	25 *	1.87	−1.44
Mean stomatal resistance ( $s m^{-1}$ )	$r_{st}$	235 *	−13.06	19.96
Aerodynamic resistance between canopy source height and reference level ( $s m^{-1}$ )	$r_a^a$	**	4.51	−4.45
Bulk boundary layer resistance of the vegetative elements in the canopy ( $s m^{-1}$ )	$r_a^c$	**	1.87	−1.44
Aerodynamic resistance between the substrate and canopy source height ( $s m^{-1}$ )	$r_a^s$	**	1.99	−1.61
Bulk stomatal resistance of the canopy ( $s m^{-1}$ )	$r_s^c$	**	−12.82	20.3
Surface resistance of the substrate ( $s m^{-1}$ )	$r_s^s$	2000 *	−3.19	5.93
Instantaneous net radiation ( $W m^{-2}$ )	$Rn_i$	**	20.60	−20.03
Instantaneous Soil heat flux ( $W m^{-2}$ )	$G_i$	**	−2.18	2.75
Instantaneous available energy ( $W m^{-2}$ )	$A_i$	**	17.96	−17.39

\* Constant values; \*\* Computed values.

### 3.3. Spatial Variability of Actual Evapotranspiration

For flowering, pit hardening and fruit colouring, maps of the actual evapotranspiration were generated using the temporal variability of  $ET_{SW}$  within the drip-irrigated olive orchard (Figure 5). While differences were observed in the  $ET_{SW}$  values over the entire time series (from 1.34 to 3.69 mm), the spatial variability for each of these days was low, with a maximum variation between 2.85 and 3.07 mm d<sup>-1</sup> (DOY 22). These low variations of the spatially distributed  $ET_{SW}$  maps could be associated with the low intra-orchard spatial variability of  $A_i$  (Figure 6), which presented a standard deviation between 3 and 6 W m<sup>-2</sup> for the entire study period. The highest value of  $A_i$  was observed on DOY 339 when the  $A_i$  ranged between 476 and 494 W m<sup>-2</sup>. On the other hand, when we consider the daily variation, the results reflected a low spatial variability of the available energy. These results are logical when considering that the orchard presents similar management conditions (irrigation practices, training systems, canopy management, fertilization, among others), which are expressed by the low spatial variability at the experimental site.

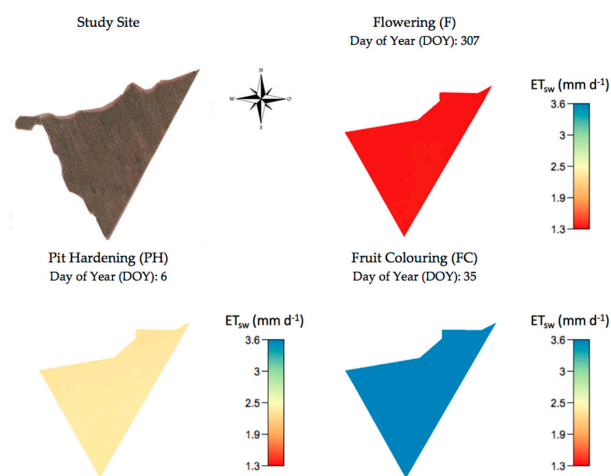


**Figure 5.** Maps of daily actual evapotranspiration (ET) computed from the SW model using remote sensing and meteorological data.

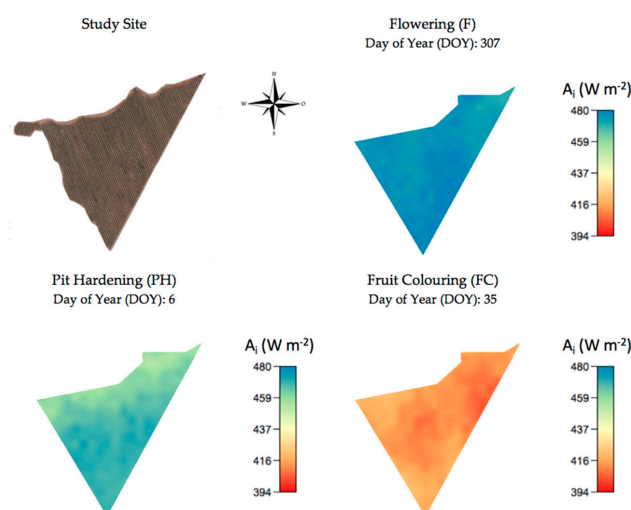


**Figure 6.** Maps of instantaneous Available energy ( $A_i$ ) generated from satellite images and ground-based climate data.

#### 4. Final Remarks

The results that were obtained in this study were similar to those that were reported in the literature for estimating olive ET when using the traditional approach of SW model [24,26,27]. This approach, however, does not include satellite images to account for the spatial variability of ET. For the main phenological stages, this study suggested that the SW model that uses satellite images and meteorological data could be suitable to estimate olive ET on a pixel-by-pixel basis. For practical application, however, the SW model requires good parameterizations of  $r_{st}$  and LAI, which are included in the formulation of  $r_s^c$ . According to Ortega-Farías and Lopez-Olivari [24], the parameterization of  $r_s^c$  depends on the canopy characteristics, which are mainly expressed by the training system and plant water status. In this study, the canopy architecture was maintained almost constant during the study with values of LAI and  $f_c$  ranging between 1.16–1.38  $m^2 m^{-2}$  and 0.26–0.3, respectively. Also, the drip-irrigated olive orchard was maintained under non-water stress conditions ( $\Psi_{md} > -1.49$  MPa), indicating that the constant value of stomatal resistance ( $235 \pm 60.84 s m^{-1}$ ) used in the SW model was adequate. However, commercial olive orchards that possess different training systems, tree water status, and canopy sizes require the incorporation of spatially distributed values of LAI and stomatal conductance to increase the accuracy of the SW model to simulate ET. To accomplish this task, it is necessary to evaluate sub-models for predicting the spatial variability of  $A_i$ , LAI, and  $r_s^c$  of olive orchards with different canopy geometry and tree water status. Finally, the results of this study suggested that the SW model could be used to estimate olive ET as a complement to the satellite-based remote sensing (SBRs) models, like METRIC.

#### 5. Conclusions

Results of this study suggested that the SW model could be a potential tool to compute spatial the variability of olive ET when using satellite images and ground-based climate data. In this case,  $Rn_i$  and  $G_i$  were obtained from satellite information and were introduced to the SW model through  $A_i$ . Simulated values of  $LE_i$ ,  $Rn_i$ ,  $G_i$ , and  $A_i$  were generally in good agreement with ground-based measurements within the olive orchard. In this case, the errors and RMSE ranged between 4% and 12% of observed values and 25–39  $W m^{-2}$ , respectively. For daily water consumption, the results indicated that the SW model was able to predict olive ET with errors of 10% and RMSE = 0.3  $mm d^{-1}$ . The observed results were consistent with the literature and are within the acceptable range for applications of remote sensing models in agriculture. Furthermore, the results also encourage the continued testing of this methodology in heterogeneous (vineyards and orchards) canopies with the aim of evaluating the effect of intra-orchard spatial variabilities of soil and canopy vigor on the estimation of ET. However, the practical application of the SW model requires adequate parameterizations of  $r_{st}$  and LAI of olive orchards under different training and system.

**Acknowledgments:** This study was supported by the Chilean government through the projects FONDECYT (No. 1130729) and FONDEF (No. D10I1157) and by the Universidad de Talca through the research program “Adaptation of Agriculture to Climate Change (A2C2)”. The authors would like to thank Manuel Barrera and Alvaro Ried from the “Oliveros de Quepu” Company for their technical support.

**Author Contributions:** Fernando Fuentes-Peñailillo and Samuel Ortega-Farías conceived and designed the experiments, supported the statistical analysis, and wrote the original manuscript draft. Cesar Acevedo-Opazo and David Fonseca-Luengo contributed extensively to results interpretation and discussions and editing of the manuscript.

**Conflicts of Interest:** The authors declare no conflict of interest.

#### List of Symbols

$A_i$	Instantaneous available energy leaving the complete canopy ( $W m^{-2}$ )
$A_{Si}$	Available energy at the soil surface ( $W m^{-2}$ )
$A_w$	Percentage of wetted area (%)

b	Ratio of estimated to observed values (dimensionless)
B	Bowen ratio (dimensionless)
$C_C$	Canopy resistance coefficient (dimensionless)
$C_S$	Soil surface resistance coefficient (dimensionless)
C	Extinction coefficient of crop for net radiation (dimensionless)
$C_P$	Specific heat of the air at constant pressure ( $1013 \text{ J kg}^{-1} \text{ }^\circ\text{K}^{-1}$ )
CV	Coefficient of variation (%)
d	Zero plane displacement of crop with complete canopy cover ( $\text{LAI} = 4$ ) (m)
$D_i$	Water vapor pressure deficit at the reference height (kPa)
$E_i$	Latent heat flux from soil evaporation ( $\text{W m}^{-2}$ )
$E_F$	Reference evapotranspiration fraction (dimensionless)
ET	Daily actual evapotranspiration ( $\text{mm d}^{-1}$ )
$\text{ET}_{\text{EC}}$	Daily actual evapotranspiration obtained from de eddy covariance (EC) method ( $\text{mm d}^{-1}$ )
$\text{ET}_i$	Instantaneous actual evapotranspiration computed from the Shuttleworth and Wallace (SW) model ( $\text{mm h}^{-1}$ )
$\text{ET}_o$	Reference evapotranspiration ( $\text{mm d}^{-1}$ )
$\text{ET}_{oi}$	Instantaneous reference evapotranspiration ( $\text{mm h}^{-1}$ )
$\text{ET}_{\text{sw}}$	Daily actual evapotranspiration estimated using the SW model ( $\text{mm d}^{-1}$ )
fc	Fractional crop cover (dimensionless)
G	Soil heat flux ( $\text{W m}^{-2}$ )
$G_i$	Instantaneous soil heat flux ( $\text{W m}^{-2}$ )
H	Sensible heat flux ( $\text{W m}^{-2}$ )
$H_B$	H corrected using the Bowen ratio approach ( $\text{W m}^{-2}$ )
$I_a$	Index of agreement (dimensionless)
Kc	Crop coefficient (dimensionless)
Kcb	basal crop coefficient (dimensionless)
Ke	soil evaporation coefficient (dimensionless)
LAI	Leaf area index ( $\text{m}^2 \text{ m}^{-2}$ )
$\text{LE}_{\text{EC}}$	Latent heat flux obtained from the EC method ( $\text{W m}^{-2}$ )
$\text{LE}_B$	Instantaneous LE corrected using the Bowen ratio approach ( $\text{W m}^{-2}$ )
$\text{LE}_i$	Instantaneous LE estimated using SW ( $\text{W m}^{-2}$ )
MAE	Mean absolute error (dimensionless)
N	Total number of observations,
n	Eddy diffusivity decay constant in crop with complete canopy crop cover (dimensionless)
$O_i$	Observed values ( $\text{W m}^{-2}$ or $\text{mm d}^{-1}$ )
$\bar{O}$	Mean of the observed values ( $\text{W m}^{-2}$ or $\text{mm d}^{-1}$ )
$P_i$	Estimated values ( $\text{W m}^{-2}$ or $\text{mm d}^{-1}$ )
Pp	precipitation (mm)
RH	Relative air humidity (%)
Rn	Net radiation ( $\text{W m}^{-2}$ )
$\text{Rn}_{\text{avg}}$	Average daily values of net radiation ( $\text{W m}^2$ )
$\text{Rn}_i$	Instantaneous net radiation ( $\text{W m}^2$ )
$\text{Rn}_{\text{Si}}$	Instantaneous net radiation on the surface of the ground ( $\text{W m}^{-2}$ )
$R_{s\downarrow}$	Incident short-wave radiation ( $\text{W m}^{-2}$ )
$R_{L\downarrow}$	Incoming long-wave radiation ( $\text{W m}^{-2}$ )
$R_{L\uparrow}$	Outgoing long-wave radiation ( $\text{W m}^{-2}$ )
$R^2$	Coefficient of determination (dimensionless)
$r_b$	Mean boundary layer resistance per unit area of vegetation ( $\text{s m}^{-1}$ )
$r_a^c$	Bulk boundary layer resistance of the vegetative elements in the canopy ( $\text{s m}^{-1}$ )
$r_a^a$	Aerodynamic resistance between the canopy source height and reference level ( $\text{s m}^{-1}$ )
$r_s^c$	Canopy resistance ( $\text{s m}^{-1}$ )
$r_a^s$	Aerodynamic resistance between the soil and canopy source height ( $\text{s m}^{-1}$ )
$r_s^s$	Soil surface resistance ( $\text{s m}^{-1}$ )
$r_{\text{st}}$	Mean stomatal resistance ( $\text{s m}^{-1}$ )



T <sub>a</sub>	Air temperature (°C)
T <sub>avg</sub>	Average daily values of temperature (°C)
T <sub>i</sub>	Latent heat flux from the olive transpiration (W m <sup>-2</sup> )
T <sub>s</sub>	Superficial temperature (°K)
T <sub>n</sub>	Near surface air temperature (°K)
u	Wind speed (m s <sup>-1</sup> )
u <sub>avg</sub>	Average daily values of wind speed (m s <sup>-1</sup> )
Z <sub>om</sub>	Surface roughness (m)
z <sub>o</sub>	Roughness length of crop with complete canopy cover (s m <sup>-1</sup> )
z <sub>ó</sub>	Roughness length of soil surface (s m <sup>-1</sup> )
α	Surface albedo (dimensionless)
α <sub>i</sub>	Instantaneous surface albedo (dimensionless)
ε <sub>a</sub>	Effective atmospheric emissivity (dimensionless)
ε <sub>0</sub>	Superficial emissivity (dimensionless)
λ	Latent heat of vaporization (1013 MJ kg <sup>-1</sup> ),
ρ <sub>w</sub>	Water density (1000 kg m <sup>-3</sup> ),
σ	Stefan-Boltzmann constant (5.67 × 10 <sup>-8</sup> Wm <sup>-2</sup> °K <sup>-4</sup> )
γ	Psychrometric constant (kPa °K <sup>-1</sup> )
τ <sub>sw</sub>	Wide-band atmospheric transmissivity (dimensionless)
Ψ <sub>md</sub>	Midday stem water potential (MPa)
Δ	Slope of the saturation vapor pressure curve at the mean temperature (kPa °C <sup>-1</sup> )

## References

- Ortega-Farías, S.; Irmak, S.; Cuenca, R.H. Special issue on evapotranspiration measurement and modeling. *Irrig. Sci.* **2009**, *28*, 1–3. [\[CrossRef\]](#)
- Fereres, E.; Soriano, M.A. Deficit irrigation for reducing agricultural water use. *J. Exp. Bot.* **2007**, *58*, 147–159. [\[CrossRef\]](#) [\[PubMed\]](#)
- Allen, R.G.; Pereira, L.S.; Raes, D.; Smith, M. *Crop Evapotranspiration—Guidelines for Computing Crop Water Requirements—FAO Irrigation and Drainage Paper 56*; Food and Agriculture Organization of the United Nations (FAO): Rome, Italy, 1998.
- Er-Raki, S.; Chehbouni, A.; Boulet, G.; Williams, D.G. Using the dual approach of FAO-56 for partitioning ET into soil and plant components for olive orchards in a semi-arid region. *Agric. Water Manag.* **2010**, *97*, 1769–1778. [\[CrossRef\]](#)
- Er-Raki, S.; Chehbouni, A.; Duchemin, B. Combining Satellite Remote Sensing Data with the FAO-56 Dual Approach for Water Use Mapping in Irrigated Wheat Fields of a Semi-Arid Region. *Remote Sens.* **2010**, *2*, 375–387. [\[CrossRef\]](#)
- Cammalleri, C.; Ciraolo, G.; Minacapilli, M.; Rallo, G. Evapotranspiration from an Olive Orchard using Remote Sensing-Based Dual Crop Coefficient Approach. *Water Resour. Manag.* **2013**, *27*, 4877–4895. [\[CrossRef\]](#)
- Paço, T.A.; Pocas, I.; Cunha, M.; Silvestre, J.C.; Santos, F.L.; Paredes, P.; Pereira, L.S. Evapotranspiration and crop coefficients for a super intensive olive orchard. An application of SIMDualKc and METRIC models using ground and satellite observations. *J. Hydrol.* **2014**, *519*, 2067–2080. [\[CrossRef\]](#)
- Martínez-Cob, A.; Faci, J.M. Evapotranspiration of an hedge-pruned olive orchard in a semiarid area of NE Spain. *Agric. Water Manag.* **2010**, *97*, 410–418. [\[CrossRef\]](#)
- Lopez-Olivari, R.; Ortega-Farías, S.; Poblete-Echeverría, C. Partitioning of net radiation and evapotranspiration over a superintensive drip-irrigated olive orchard. *Irrig. Sci.* **2016**, *34*, 17–31. [\[CrossRef\]](#)
- Allen, R.G.; Pereira, L.S. Estimating crop coefficients from fraction of ground cover and height. *Irrig. Sci.* **2009**, *28*, 17–34. [\[CrossRef\]](#)
- Pôças, I.; Paco, T.A.; Paredes, P.; Cunha, M.; Pereira, L.S. Estimation of Actual Crop Coefficients Using Remotely Sensed Vegetation Indices and Soil Water Balance Modelled Data. *Remote Sens.* **2015**, *7*, 2373–2400. [\[CrossRef\]](#)

12. Er-Raki, S.; Chehbouni, A.; Hoedjes, J.; Ezzahar, J.; Duchemin, B.; Jacob, F. Improvement of FAO-56 method for olive orchards through sequential assimilation of thermal infrared-based estimates of ET. *Agric. Water Manag.* **2008**, *95*, 309–321. [[CrossRef](#)]
13. Anadranistakis, M.; Liakatas, A.; Kerkides, P.; Rizos, S.; Gavanosis, J.; Poulouvassilis, A. Crop water requirements model tested for crops grown in Greece. *Agric. Water Manag.* **2000**, *45*, 297–316. [[CrossRef](#)]
14. Ortega-Farías, S.; Poblete-Echeverría, C.; Brisson, N. Parameterization of a two-layer model for estimating vineyard evapotranspiration using meteorological measurements. *Agric. For. Meteorol.* **2010**, *150*, 276–286. [[CrossRef](#)]
15. Testi, L.; Villalobos, F.J.; Orgaz, F. Evapotranspiration of a young irrigated olive orchard in southern Spain. *Agric. For. Meteorol.* **2004**, *121*, 1–18. [[CrossRef](#)]
16. Were, A.; Villagarcía, L.; Domingo, F.; Moro, M.J.; Dolman, A.J. Aggregating spatial heterogeneity in a bush vegetation patch in semi-arid SE Spain: A multi-layer model versus a single-layer model. *J. Hydrol.* **2008**, *349*, 156–167. [[CrossRef](#)]
17. Zhou, M.C.; Ishidaira, H.; Hapuarachchi, H.P.; Magome, J.; Kiem, A.S.; Takeuchi, K. Estimating potential evapotranspiration using Shuttleworth–Wallace model and NOAA-AVHRR NDVI data to feed a distributed hydrological model over the Mekong River basin. *J. Hydrol.* **2006**, *327*, 151–173. [[CrossRef](#)]
18. Kato, T.; Kamichika, M. Determination of a crop coefficient for evapotranspiration in a sparse sorghum field. *Irrig. Drain.* **2006**, *55*, 165–175. [[CrossRef](#)]
19. Gardiol, J.M.; Serio, L.A.; Della Maggiora, A.I. Modelling evapotranspiration of corn (*Zea mays*) under different plant densities. *J. Hydrol.* **2003**, *271*, 188–196. [[CrossRef](#)]
20. Zhang, B.; Kang, S.; Li, F.; Zhang, L. Comparison of three evapotranspiration models to Bowen ratio-energy balance method for a vineyard in an arid desert region of northwest China. *Agric. For. Meteorol.* **2008**, *148*, 1629–1640. [[CrossRef](#)]
21. Ortega-Farías, S.; Carrasco, M.; Oliosio, A.; Acevedo, C.; Poblete, C. Latent heat flux over Cabernet Sauvignon vineyard using the Shuttleworth and Wallace model. *Irrig. Sci.* **2006**, *25*, 161–170. [[CrossRef](#)]
22. Zhang, B.; Kang, S.; Zhang, L.; Tong, L.; Du, T.; Li, F.; Zhang, J. An evapotranspiration model for sparsely vegetated canopies under partial root-zone irrigation. *Agric. For. Meteorol.* **2009**, *149*, 2007–2011. [[CrossRef](#)]
23. Zhao, P.; Li, S.; Li, F.; Du, T.; Tong, L.; Kang, S. Comparison of dual crop coefficient method and Shuttleworth–Wallace model in evapotranspiration partitioning in a vineyard of northwest China. *Agric. Water Manag.* **2015**, *160*, 41–56. [[CrossRef](#)]
24. Ortega-Farías, S.; Lopez-Olivari, R. Validation of a Two-Layer Model to Estimate Latent Heat Flux and Evapotranspiration in a Drip-Irrigated Olive Orchard. *Trans. ASABE* **2012**, *55*, 1169–1178. [[CrossRef](#)]
25. Brenner, A.J.; Incoll, L.D. The effect of clumping and stomatal response on evaporation from sparsely vegetated shrublands. *Agric. For. Meteorol.* **1997**, *84*, 187–205. [[CrossRef](#)]
26. Ortega-Farías, S.; Ortega-Salazar, S.; Poblete, T.; Kilic, A.; Allen, R.; Poblete-Echeverría, C.; Ahumada-Orellana, L.; Zuniga, M.; Sepulveda, D. Estimation of energy balance components over a drip-irrigated olive orchard using thermal and multispectral cameras placed on a helicopter-based unmanned aerial vehicle (UAV). *Remote Sens.* **2016**, *8*, 638. [[CrossRef](#)]
27. Ortega-Farías, S.; Ortega-Salazar, S.; Aguilar, R.; De la Fuente, D.; Fuentes, F. Evaluation of a model to estimate net radiation over a drip-irrigated olive orchard using landsat satellite images. *Acta Hortic.* **2014**, *1057*, 309–314. [[CrossRef](#)]
28. Carrasco-Benavides, M.; Ortega-Farías, S.; Lagos, L.O.; Kleissl, J.; Morales-Salinas, L.; Kilic, A. Parameterization of the satellite-based model (METRIC) for the estimation of instantaneous surface energy balance components over a drip-irrigated vineyard. *Remote Sens.* **2011**, *6*, 11342–11371. [[CrossRef](#)]
29. Cuenca, R.H.; Ciotti, S.P.; Hagimoto, Y. Application of Landsat to Evaluate Effects of Irrigation Forbearance. *Remote Sens.* **2011**, *5*, 3776–3802. [[CrossRef](#)]
30. Long, D.; Singh, V.P. A modified surface energy balance algorithm for land (M-SEBAL) based on a trapezoidal framework. *Water Resour. Res.* **2012**, *48*. [[CrossRef](#)]
31. Long, D.; Singh, V.P. Assessing the impact of end-member selection on the accuracy of satellite-based spatial variability models for actual evapotranspiration estimation. *Water Resour. Res.* **2013**, *49*, 2601–2618. [[CrossRef](#)]

32. Dhungel, R.; Allen, R.G.; Trezza, R.; Robison, C.W. Comparison of Latent Heat Flux Using Aerodynamic Methods and Using the Penman-Monteith Method with Satellite-Based Surface Energy Balance. *Remote Sens.* **2014**, *6*, 8844–8877. [[CrossRef](#)]
33. Tognetti, R.; D'Andria, R.; Sacchi, R.; Lavini, A.; Morelli, G.; Alvino, A. Deficit irrigation affects seasonal changes in leaf physiology and oil quality of *Olea europaea* (cultivars Frantoio and Leccino). *Ann. Appl. Biol.* **2007**, *150*, 169–186. [[CrossRef](#)]
34. Pérez-López, D.; Gijón, M.C.; Marino, J.; Moriana, A. Water relation response to soil chilling of six olive (*Olea europaea* L.) cultivars with different frost resistance. *Span. J. Agric. Res.* **2010**, *8*, 780–789. [[CrossRef](#)]
35. Dichio, B.; Xiloyannis, C.; Sofo, A.; Montanaro, G. Osmotic regulation in leaves and roots of olive trees during a water deficit and rewatering. *Tree Physiol.* **2006**, *26*, 179–185. [[CrossRef](#)] [[PubMed](#)]
36. Poblete-Echeverría, C.; Sepúlveda-Reyes, D.; Ortega-Farías, S. Effect of height and time lag on the estimation of sensible heat flux over a drip-irrigated vineyard using the surface renewal (SR) method across distinct phenological stages. *Agric. Water Manag.* **2014**, *141*, 74–83. [[CrossRef](#)]
37. Shao, C.; Chen, J.; Li, L.; Xu, W.; Chen, S.; Gwen, T.; Xu, J.; Zhang, W. Spatial variability in soil heat flux at three Inner Mongolia steppe ecosystems. *Agric. For. Meteorol.* **2008**, *148*, 1433–1443. [[CrossRef](#)]
38. Schotanus, P.; Nieuwstadt, F.T.M.; de Bruin, H.A.R. Temperature measurement with a sonic anemometer and its application to heat and moisture fluxes. *Bound.-Layer Meteorol.* **1983**, *26*, 81–93. [[CrossRef](#)]
39. Webb, E.K.; Pearman, G.I.; Leuning, R. Correction of flux measurements for density effects due to heat and water vapour transfer. *Q. J. R. Meteorol. Soc.* **1980**, *106*, 85–100. [[CrossRef](#)]
40. Twine, T.E.; Kustas, W.P.; Norman, J.M.; Cook, D.R. Correcting eddy-covariance flux underestimates over a grassland. *Agric. For. Meteorol.* **2000**, *103*, 279–300. [[CrossRef](#)]
41. Shuttleworth, W.J.; Wallace, J.S. Evaporation from sparse crops—An energy combination theory. *Q. J. R. Meteorol. Soc.* **1985**, *111*, 839–855. [[CrossRef](#)]
42. Allen, R.G.; Tasumi, M.; Trezza, R. Satellite-based energy balance for mapping evapotranspiration with internalized calibration (METRIC)—Model. *J. Irrig. Drain. Eng.* **2007**, *133*, 380–394. [[CrossRef](#)]
43. Storey, J.; Scaramuzza, P.; Schmidt, G.; Barsi, J. Landsat 7 scan line corrector-off gap-filled product development. In Proceedings of the Pecora 16 Global Priorities in Land Remote Sensing, Sioux Falls, SD, USA, 23–27 October 2005.
44. Zeng, C.; Shen, H.; Zhang, L. Recovering missing pixels for Landsat ETM plus SLC-off imagery using multi-temporal regression analysis and a regularization method. *Remote Sens. Environ.* **2013**, *131*, 182–194. [[CrossRef](#)]
45. Spiliotopoulos, M.; Holden, N.M.; Loukas, A. Mapping evapotranspiration coefficients in a temperate maritime climate using the metric model and landsat TM. *Water* **2017**, *9*, 23. [[CrossRef](#)]
46. Reyes-González, A.; Kjaersgaard, J.; Trooien, T.; Hay, C.; Ahiablame, L. Comparative Analysis of METRIC Model and Atmometer Methods for Estimating Actual Evapotranspiration. *Int. J. Agron.* **2017**, *2017*, 3632501. [[CrossRef](#)]
47. Jimenez-Bello, M.A.; Castel, J.R.; Testi, L.; Intrigliolo, D.S. Assessment of a Remote Sensing Energy Balance Methodology (SEBAL) Using Different Interpolation Methods to Determine Evapotranspiration in a Citrus Orchard. *IEEE J. Sel. Top. Appl. Earth Obs. Remote Sens.* **2015**, *8*, 1465–1477. [[CrossRef](#)]
48. Song, L.; Liu, S.; Kustas, W.P.; Zhou, J.; Xu, Z.; Xia, T.; Li, M. Application of remote sensing-based two-source energy balance model for mapping field surface fluxes with composite and component surface temperatures. *Agric. For. Meteorol.* **2016**, *230*, 8–19. [[CrossRef](#)]
49. Serra, P.; Salvati, L.; Queral, E.; Pin, C.; Gonzalez, O.; Pons, X. Estimating Water Consumption and Irrigation Requirements in a Long-Established Mediterranean Rural Community by Remote Sensing and Field Data. *Irrig. Drain.* **2016**, *65*, 578–588. [[CrossRef](#)]
50. Mayer, D.G.; Butler, D.G. Statistical validation. *Ecol. Model.* **1993**, *68*, 21–32. [[CrossRef](#)]
51. Willmott, C.J.; Ackleson, S.G.; Davis, R.E.; Feddema, J.J.; Klink, K.M.; Legates, D.R.; O'Donnell, J.; Rowe, C.M. Statistics for the Evaluation and Comparison of Models. *J. Geophys. Res. Oceans* **1985**, *90*, 8995–9005. [[CrossRef](#)]
52. Williams, D.G.; Cable, W.; Hultine, K.; Hoedjes, J.; Yezpe, E.A.; Simonneaux, V.; Er-Raki, S.; Boulet, G.; de Bruin, H.; Chehbouni, A.; et al. Evapotranspiration components determined by stable isotope, sap flow and eddy covariance techniques. *Agric. For. Meteorol.* **2004**, *125*, 241–258. [[CrossRef](#)]

53. Ezzahar, J.; Chehbouni, A.; Hoedjes, J.C.B.; Er-Raki, S.; Chehbouni, A.; Boulet, G.; Bonnefond, J.M.; de Bruin, H.A.R. The use of the scintillation technique for monitoring seasonal water consumption of olive orchards in a semi-arid region. *Agric. Water Manag.* **2007**, *89*, 173–184. [[CrossRef](#)]
54. Villalobos, F.J.; Testi, L.; Orgaz, F.; García-Tejera, O.; López-Bernal, Á.; Victoria Gonzalez-Dugo, M.; Ballester-Lurbe, C.; Ramon Castel, J.; Jose Alarcon-Cabanero, J.; Nicolas-Nicolas, E.; et al. Modelling canopy conductance and transpiration of fruit trees in Mediterranean areas: A simplified approach. *Agric. For. Meteorol.* **2013**, *171*, 93–103. [[CrossRef](#)]
55. Testi, L.; Villalobos, F.J.; Orgaz, F.; Fereres, E. Water requirements of olive orchards: I simulation of daily evapotranspiration for scenario analysis. *Irrig. Sci.* **2006**, *24*, 69–76. [[CrossRef](#)]
56. Lee, X.; Black, T.A. Atmospheric turbulence within and above a douglas-fir stand. Part II: Eddy fluxes of sensible heat and water vapour. *Bound.-Layer Meteorol.* **1993**, *64*, 369–389. [[CrossRef](#)]
57. Wilson, K.; Goldstein, A.; Falge, E.; Aubinet, M.; Baldocchi, D.; Berbigier, P.; Bernhofer, C.; Ceulemans, R.; Dolman, H.; Field, C.; et al. Energy balance closure at FLUXNET sites. *Agric. For. Meteorol.* **2002**, *113*, 223–243. [[CrossRef](#)]
58. Leuning, R.; van Gorsel, E.; Massman, W.J.; Isaac, P.R. Reflections on the surface energy imbalance problem. *Agric. For. Meteorol.* **2012**, *156*, 65–74. [[CrossRef](#)]
59. Allen, R.G.; Pereira, L.S.; Howell, T.A.; Jensen, M.E. Evapotranspiration information reporting: I. Factors governing measurement accuracy. *Agric. Water Manag.* **2011**, *98*, 899–920. [[CrossRef](#)]
60. Liu, H.; Foken, T. A modified Bowen ratio method to determine sensible and latent heat fluxes. *Meteorol. Z.* **2001**, *10*, 71–80. [[CrossRef](#)]
61. De Teixeira, A.H.C.; Bastiaanssen, W.G.M.; Ahmad, M.D.; Bos, M.G. Reviewing SEBAL input parameters for assessing evapotranspiration and water productivity for the Low-Middle São Francisco River basin, Brazil. *Agric. For. Meteorol.* **2009**, *149*, 462–476. [[CrossRef](#)]
62. Liu, S.; Lu, L.; Mao, D.; Jia, L. Evaluating parameterizations of aerodynamic resistance to heat transfer using field measurements. *Hydrol. Earth Syst. Sci.* **2007**, *11*, 769–783. [[CrossRef](#)]



© 2018 by the authors. Licensee MDPI, Basel, Switzerland. This article is an open access article distributed under the terms and conditions of the Creative Commons Attribution (CC BY) license (<http://creativecommons.org/licenses/by/4.0/>).